0026-895X/09/7605-957–968$20.00
MOLECULAR PHARMACOLOGY
Vol. 76, No. 5
58180/3528771
Mol Pharmacol 76:957–968, 2009
Printed in U.S.A.

Targeting of the Akt-Nuclear Factor-κB Signaling Network by [1-(4-Chloro-3-nitrobenzenesulfonyl)-1*H*-indol-3-yl]-methanol (OSU-A9), a Novel Indole-3-Carbinol Derivative, in a Mouse Model of Hepatocellular Carcinoma[S]

Hany A. Omar, Aaron M. Sargeant, Jing-Ru Weng, Dasheng Wang, Samuel K. Kulp, Tushar Patel, and Ching-Shih Chen

Division of Medicinal Chemistry, College of Pharmacy (H.A.O., A.M.S., D.W., S.K.K., C.S.C.) and Division of Gastroenterology, Hepatology, and Nutrition, Department of Internal Medicine (TP), the Ohio State University, Columbus, Ohio; and Department of Biological Science and Technology, China Medical University, Taichung, Taiwan (J.R.W.)

Received May 28, 2009; accepted August 25, 2009

ABSTRACT

Constitutive activation of Akt and nuclear factor-κB (NF-κB) represents major cellular abnormalities associated with the development and progression of hepatocellular carcinoma (HCC). Based on the structure of indole-3-carbinol, a chemopreventive phytochemical, we developed a novel derivative, [1-(4-chloro-3-nitrobenzenesulfonyl)-1*H*-indol-3-yl]-methanol (OSU-A9), that exhibits higher potency in inducing apoptosis by targeting the Akt-NF-κB signaling network. This study was aimed at assessing the antitumor activity of OSU-A9 using both in vitro and in vivo models of HCC, a malignancy in which the Akt-NF-κB signaling network plays major roles in pathogenesis and therapeutic resistance. Our data show that OSU-A9 was 100 times more potent than indole-3-carbinol in suppressing the viability of Hep3B, Huh7, and PLC5 HCC cells with IC_{50} values ranging from 2.8 to 3.2 μM. OSU-A9 interfered with the interplay between Akt- and NF-κB-mediated oncogenic signaling, leading to changes in the functional status of diverse signaling effectors involved in cell cycle progression, apoptosis, angiogenesis, and metastasis. The in vivo efficacy of OSU-A9 was assessed in nude mice bearing luciferase-expressing Hep3B xenograft tumors. Daily oral treatments with OSU-A9 at 25 or 50 mg/kg for 56 days suppressed tumor growth by 67 and 80%, respectively, which was correlated with changes in intratumoral biomarkers pertinent to Akt-NF-κB signaling, and without apparent toxicity or evidence of hepatic biotransformation enzyme induction. Together, these findings indicate that OSU-A9 is a potent, orally bioavailable inhibitor of the Akt-NF-κB signaling network with a broad spectrum of antitumor activity that includes targets regulating multiple aspects of HCC pathogenesis and progression.

Hepatocellular carcinoma (HCC), the most common type of malignant primary liver tumor, is the third most frequent cause of cancer death worldwide (El-Serag and Rudolph, 2007). The clinical management of HCC is complicated by late-stage disease at presentation and prevalent underlying liver dysfunction that renders most patients ineligible for potentially curative surgical therapies, which are generally suitable for only 20 to 30% of patients (Blum, 2005). Moreover, intrinsic resistance to chemotherapy contributes to the generally poor prognosis of HCC and limits the availability of effective systemic therapies (Blum, 2005). Substantial evidence indicates that this cellular resistance to chemotherapeutics is attributable to the heterogeneity of the genetic

This work was supported by the National Institutes of Health National Cancer Institute [Grants R01-CA112250, R21-CA135560] (to C.-S.C.) and the National Science Council [Grant NSC 96-2320-B-039-021-MY3] (to J.-R.W.).
Article, publication date, and citation information can be found at http://molpharm.aspetjournals.org.
doi:10.1124/mol.109.058180.
[S] The online version of this article (available at http://molpharm.aspetjournals.org) contains supplemental material.

ABBREVIATIONS: HCC, hepatocellular carcinoma; NF-κB, nuclear factor κB; IκB, inhibitor of nuclear factor-κB; SB-203580, 4-(4-fluorophenyl)-2-(4-methylsulfinylphenyl)-5-(4-pyridyl)1*H*-imidazole; DMSO, dimethyl sulfoxide; ERK, extracellular signal-regulated kinase; JNK, c-Jun N-terminal kinase; Bad, Bcl-2-associated death promoter; Akt, v-akt murine thymoma viral oncogene homolog; CXCR4, chemokine, CXC motif, receptor 4; MMP, matrix metalloproteinase; cIAP, cellular inhibitor of apoptosis protein; Bcl-2, B cell lymphoma-2; Bcl-xL, B cell lymphoma-extra large; c-Myc, cellular myelocytomatosis viral oncogene; PARP, poly(ADP-ribose) polymerase; CA, constitutively active; DMEM, Dulbecco's modified Eagle's medium; FBS, fetal bovine serum; MTT, 3-(4,5-dimethylthiazol-2-yl)-2,5-diphenyltetrazolium bromide; Hep3B-luc, luciferase-expressing Hep3B; H&E, hematoxylin and eosin; GSK, glycogen synthase kinase; IKKα, IκB kinase α; MAP, mitogen-activated protein kinase; TNF, tumor necrosis factor.

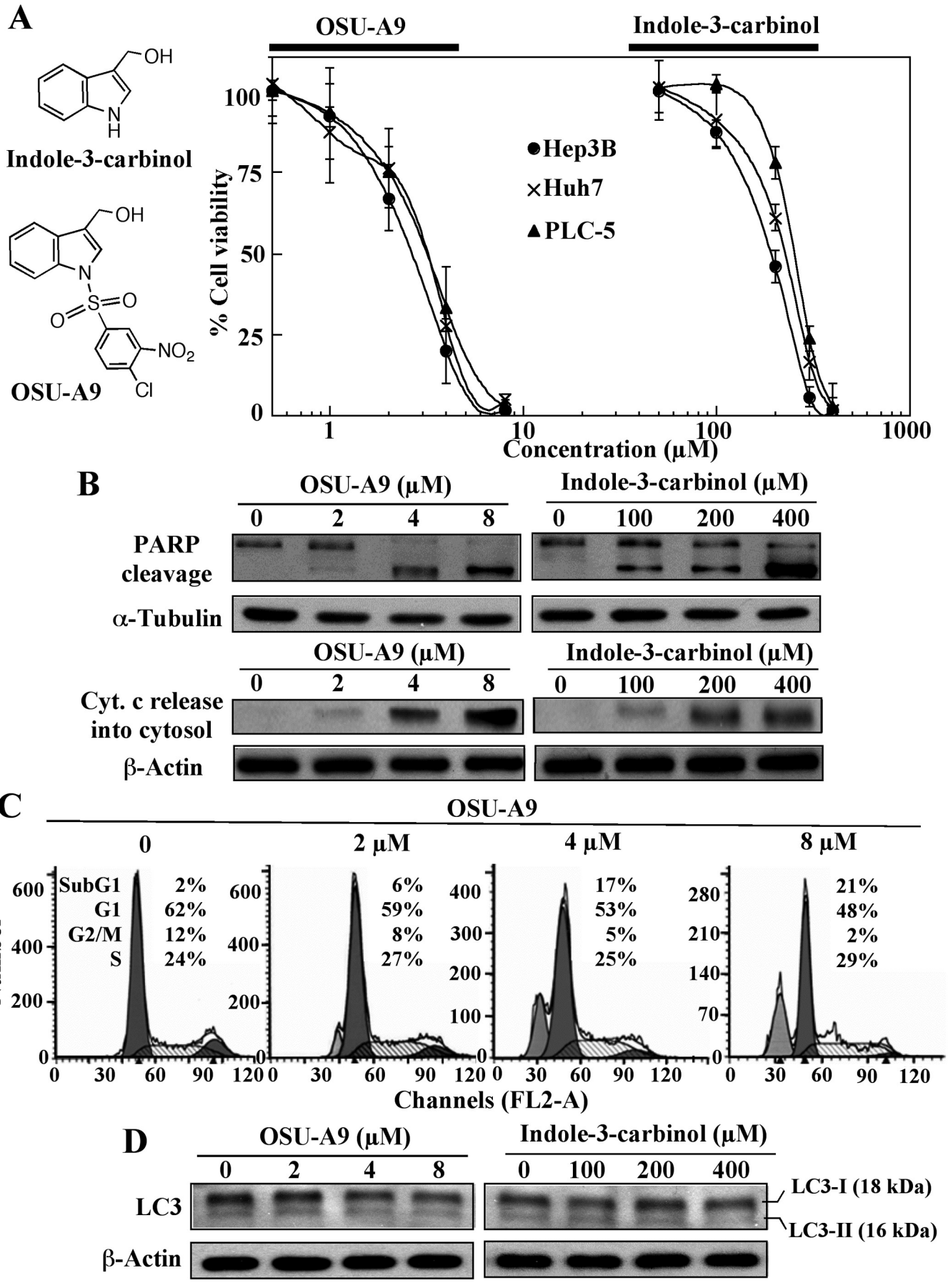

abnormalities acquired during the course of hepatocarcinogenesis, many of which dysregulate signaling pathways governing cell proliferation and survival. Among various molecular defects that allow HCC cells to evade drug-induced apoptosis signaling, constitutive activation of Akt (Hu et al., 2003; Nakanishi et al., 2005) and nuclear factor κB (NF-κB) (Arsura and Cavin, 2005) are especially noteworthy. Activation of Akt signaling has been reported in 40 to 60% of human HCC (Hu et al., 2003; Nakanishi et al., 2005), whereas NF-κB plays a key role in the tumorigenesis and progression of HCC and other inflammation-linked cancers (Arsura and Cavin, 2005; Karin, 2006), in part, by enabling malignant cells to resist apoptosis-based tumor surveillance mechanisms (Karin, 2006). Consequently, targeting signaling pathways mediated by either Akt or NF-κB, directly or indirectly, represents a viable strategy to improve therapeutic outcome in patients with HCC. The proof of principle of this premise is the survival benefit provided by treatment with the multikinase inhibitor sorafenib in patients with advanced HCC (Scanga and Kowdley, 2009). Moreover, the proteasome inhibitor bortezomib is currently undergoing a clinical trial in combination with doxorubicin in patients with HCC based on its ability to decrease the transcriptional activity of NF-κB by blocking the degradation of its inhibitor IκB (http://clinicaltrials.gov/ct2/show/NCT00083226).

The chemopreventive potential of the phytochemical indole-3-carbinol has recently received much attention because of its unique ability to perturb Akt- and NF-κB-mediated oncogenic signaling, albeit with low potency (Chinni and Sarkar, 2002; Rahman et al., 2004; Weng et al., 2007). However, the in vivo efficacy of indole-3-carbinol is limited by many factors, including low antitumor potency, limited bioavailability, and complicated pharmacokinetic behaviors due to intrinsic metabolic instability (Weng et al., 2008). Consequently, we embarked on the structural optimization of indole-3-carbinol, which yielded OSU-A9, a novel derivative that provides considerable therapeutic advantage over the parent compound because of its greater antitumor efficacy and metabolic stability (Weng et al., 2007). Among the many effects of OSU-A9 on signaling molecules that we have identified in prostate cancer cells were the suppression of Akt phosphorylation and NF-κB expression (Weng et al., 2007). Consequently, in this study, we investigated the activity of OSU-A9 against Akt- and NF-κB-mediated signaling pathways in HCC, a malignancy in which the Akt-NF-κB signaling network plays major roles in pathogenesis and therapeutic resistance. Here, we show that OSU-A9 exhibits up to 100-fold greater in vitro efficacy relative to indole-3-carbinol in HCC cells. Mechanistic evidence indicates that OSU-A9, in a manner similar to that of indole-3-carbinol, mediated its antitumor effect by blocking the Akt-NF-κB signaling network, leading to the inhibition of signaling pathways governing cell cycle progression, survival, and metastasis. Equally important, oral administration of OSU-A9 suppressed HCC xenograft tumor growth in mice without causing overt signs of toxicity.

Materials and Methods

Reagents. Indole-3-carbinol and OSU-A9 were synthesized as described previously (Weng et al., 2007). The p38 kinase inhibitor SB-203580 was purchased from Calbiochem (San Diego, CA). For in vitro experiments, agents were dissolved in DMSO, diluted in culture medium, and added to cells at a final DMSO concentration of 0.1%. For in vivo studies, OSU-A9 was prepared as a suspension in vehicle (0.5% methylcellulose, 0.1% Tween 80 in sterile water) for oral administration to tumor-bearing immunocompromised mice. Antibodies against various biomarkers were obtained as follows. Akt, p-^{473}Ser Akt, p-^{308}Ser Akt, p-Bad, Bad, Foxo3a, p-Foxo3a, p-ERKs, p-JNK, JNK, p-p38, p38, cyclin D1, NF-κB (RelA), cIAP-1, cIAP-2, MMP9, IKKα, p-^{108}Ser IKKα, and Ki67 were obtained from Cell Signaling Technologies (Danvers, MA). Hemagglutinin tag, ERKs, Bcl-2, Bcl-xL, c-Myc, p27, IκB, cytochrome *c*, and chemokine, CXC motif, receptor (CXCR) 4 were obtained from Santa Cruz Biotechnology (Santa Cruz, CA). Survivin was obtained from R&D Systems (Minneapolis, MN). β-Actin was obtained from Sigma-Aldrich (St. Louis, MO). Microtubule-associated protein 1 light chain 3 (LC3) was obtained from MBL International (Woburn, MA). Mouse monoclonal anti-poly(ADP-ribose) polymerase (PARP) antibody was purchased from BD Pharmingen (San Diego, CA). The plasmid encoding constitutively active (CA)-Akt was obtained from Addgene (Cambridge, MA). The pCMVp65 and pNF-κB-Luc plasmids were kindly provided by Dr. Hung-Wen Chen (Academia Sinica, Taiwan) and Dr. Cheng-Wen Lin (China Medical University, Taichung, Taiwan). The enhanced chemiluminescence system for detection of immunoblotted proteins was from GE Healthcare (Little Chalfont, Buckinghamshire, UK). Other chemicals and reagents were obtained from Sigma-Aldrich unless otherwise mentioned.

Cell Culture. The HCC cell lines were purchased from the following sources: Huh7 (JCRB0403) was obtained from the Health Science Research Resources Bank (Osaka, Japan). Hep3B and PLC5 were obtained from the American Type Culture Collection (Manassas, VA). Cells were cultured in Dulbecco's modified Eagle's medium (DMEM; Invitrogen, Carlsbad, CA) supplemented with 10% fetal bovine serum (FBS; Invitrogen). All cells were cultured at 37°C in a humidified incubator containing 5% CO_2. Cells in log-phase growth were harvested by trypsinization for use in various assays and in vivo studies.

Cell Viability Assay. Cell viability was assessed by using the 3-(4,5-dimethylthiazol-2-yl)-2,5-diphenyltetrazolium bromide (MTT) assay in six replicates as described previously (Kulp et al., 2006) with minor modifications. In brief, cells were seeded at 4000 cells per well in 96-well flat-bottomed plates; then, 24 to 72 h later, cells were treated with OSU-A9 and/or SB-203580 at the concentrations indicated in individual figures or with DMSO in serum-free or 5% FBS-supplemented DMEM.

Flow Cytometry/Apoptosis Assays. Approximately 5×10^5 cells were plated onto 10-cm dishes and incubated at 37°C overnight. The cells were treated with DMSO or OSU-A9 at different concentrations for 48 h, collected, washed twice with PBS, and then fixed in ice-cold ethanol at −20°C overnight. After centrifugation at 400*g* for 5 min at room temperature, the cells were stained with propidium

Fig. 1. Differential effect of OSU-A9 versus indole-3-carbinol on induction of apoptosis in HCC cells. A, left, structures of OSU-A9 and indole-3-carbinol. Right, dose-dependent effect of OSU-A9 relative to indole-3-carbinol on the cell viability of Hep3B, Huh-7, and PLC-5 HCC cells. Cells were treated with OSU-A9 or indole-3-carbinol at the indicated concentrations in 5% FBS-supplemented DMEM in 96-well plates for 48 h, and cell viability was assessed by MTT assays. Points, mean; bars, S.D. ($n = 6$). B, Western blot analysis of the dose-dependent effects of OSU-A9 versus indole-3-carbinol on PARP cleavage and cytochrome *c* release into the cytoplasm in Hep3B cells after 48-h exposure in 5% FBS-supplemented DMEM. C, flow cytometric analysis of apoptosis in the Hep3B cells after treatment with DMSO vehicle or the indicated concentrations of OSU-A9 for 48 h in 5% FBS-supplemented DMEM. The drug-treated cells were fixed and stained with propidium iodide. The extent of apoptosis was assessed by quantifying sub-2N (sub-G_1) DNA by flow cytometry. The histograms are representative of two independent experiments. D, Western blot analysis of the dose-dependent effect of OSU-A9 on the conversion of LC3-II from LC3-I in Hep3B cells after 48-h exposure in 5% FBS-supplemented DMEM.

iodide (50 μg/ml) in the presence of RNase A (100 U/ml). The distribution of cells among the phases of the cell cycle was determined on a FACScort flow cytometer equipped with ModFitLT ver. 3.0 software program (Verity Software House, Topsham ME).

Immunoblotting. Lysates of HCC cells treated with OSU-A9 at the concentrations indicated in individual figures for 48 h were prepared for immunoblotting. Western blot analysis was performed as reported previously (Kulp et al., 2006). For immunoblotting of biomarkers in Hep3B-Luc tumor xenografts, tumor tissue homogenates were prepared and immunoblotting was done as described previously (Kulp et al., 2006).

Cytochrome *c* Release from Mitochondria. Mitochondrial and cytosolic fractions were prepared from Hep3B cells treated with OSU-A9 at the concentrations indicated in Fig. 1 for 48 h using a mitochondria isolation kit for cultured cells (Pierce, Rockford, Illinois) according to the manufacturer's instructions. Cytochrome *c* was detected by Western blot analysis.

NF-κB–Dependent Reporter Gene Expression Assay. One million Hep3B cells were transiently cotransfected with 2 μg of pNF-κB-Luc reporter plasmid and 0.5 μg of the *Renilla reniformis* luciferase control reporter vector (pRL-CMV; Promega, Madison, WI) using the Amaxa Nucleofector system (Lonza, Gaithersburg, MD). Transfected cells were seeded into 12-well plates and, after 24 h of culture, treated in triplicate with different concentrations of OSU-A9 or vehicle with or without 10 ng/ml TNF-α (Peprotech, Rocky Hill, NJ) for 6 h. The luciferase activities in cell lysates were determined using the Dual-Luciferase Reporter Assay System (Promega) and normalized to the constitutive *R. reniformis* luciferase activity.

Transient Transfection with Plasmids Encoding RelA and/or CA-Akt. Hep3B cells were transfected with 2 μg of pCMVp65, CA-Akt plasmids, or the empty vector using the Amaxa Nucleofector system. Cell viability was assessed 48 h after transfection using MTT assay in six replicates as mentioned above. Expression of RelA, CA-Akt, or the effectors indicated in Fig. 3 was confirmed by immunoblotting by Western blot analysis.

Migration/Invasion Assays. Assays were performed in 24-well modified Boyden chambers (8-μm pore size; Costar; Corning Life Sciences, Lowell, MA). In the migration assay, 10^5 Hep3B cells in 0.5 ml of serum-free DMEM containing the indicated concentration of OSU-A9 or DMSO were seeded into the upper chamber insert, and incubated at 37°C for 30 min. The inserts were switched to new wells containing the same concentration of OSU-A9 or DMSO in 10% FBS-supplemented DMEM, and incubated for 6 h. Cells on the upper surface of each filter were scraped off thoroughly with cotton swabs, whereas cells on the underside of the filter were fixed in 100% methanol and stained with 5% Giemsa stain (Merck, Darmstadt, Germany). For each chamber, the number of migrated cells was counted in 10 randomly chosen 200× fields. For the invasion assay, 7.5×10^4 Hep3B cells in 0.5 ml of serum-free DMEM containing the indicated concentration of OSU-A9 or DMSO were seeded onto Matrigel-coated or uncoated membranes of the upper chambers and incubated at 37°C. The lower chambers contained the same amount of OSU-A9 or DMSO in 10% FBS/DMEM. After 24 h, noninvasive cells remaining on the upper surface of the membranes were removed with a cotton swab. Cells on the lower surface of the membrane were fixed in 100% methanol and stained with 0.1% crystal violet for 10 min. The cells on each membrane were counted in 10 200× fields. Tumor cell invasion was expressed as the number of cells that had passed through the Matrigel-coated membranes.

Generation of Luciferase-Expressing Hep3B Cells. Hep3B-luc cells were generated by stable transfection with the phCMV-luc plasmid (Genlantis, San Diego, CA) containing cDNA encoding the firefly luciferase gene. Cells were transfected using the Amaxa Nucleofector system, and stable transfectants were selected by exposure to 500 μg/ml G418 (Geneticin; Invitrogen) for 4 weeks. Stable expression of luciferase was confirmed by the detection of luciferase activity using the dual luciferase assay and detection system (Promega). Confirmation that stable transfection did not alter the sensitivity of Hep3B cells to OSU-A9 was confirmed by MTT assay. Moreover, OSU-A9 had no appreciable effect on the expression level of luciferase in Hep3B-luc cells (data not shown).

In Vivo Study. Female NCr athymic nude mice (5–7 weeks of age) were obtained from the National Cancer Institute (Frederick, MD) and group-housed under conditions of constant photoperiod (12-h light/dark cycle) with ad libitum access to sterilized food and water. All experimental procedures using mice were done in accordance with protocols approved by The Ohio State University Institutional Animal Care and Use Committee.

Each mouse received 2×10^6 Hep3B-Luc cells via subcutaneous injection in a total volume of 0.1 ml of serum-free medium containing 50% Matrigel (BD Biosciences Discovery Labware, Bedford, MA). The establishment and growth of tumors were monitored by direct measurement with calipers, as well as by measurement of bioluminescence using the IVIS imaging system (Xenogen Corporation, Alameda, CA) according to a protocol similar to those described previously (Rehemtulla et al., 2000; Jenkins et al., 2003a,b; Scatena et al., 2004). The optimal time for imaging after luciferin injection was determined by generating a kinetic curve for luciferase activity as described previously (Baba et al., 2007). Mice were administered firefly luciferin via intraperitoneal injection (150 mg/kg body weight in PBS); approximately 10 min later, mice were imaged under isoflurane anesthesia. Data acquisition and analysis were achieved using the Living Image software (Xenogen). As tumors became established (mean starting tumor volume ± S.E., 105 ± 7 mm^3), mice were randomized to three groups (n = 8–10) that received the following treatments daily: 1) vehicle, 2) OSU-A9 at 25 mg/kg body weight, and 3) OSU-A9 at 50 mg/kg body weight. Tumor burdens were determined weekly using both calipers (tumor volume = $\text{width}^2 \times \text{length} \times 0.52$) and bioluminescent imaging.

Histological and Hematological Evaluations. At terminal sacrifice, blood was collected from each mouse and three samples per experimental group were submitted to The Ohio State University Veterinary Clinical Laboratory Services for evaluation of serum chemistry and hematological parameters (Suckow et al., 2001). After exsanguination at necropsy, the liver from each animal was removed and weighed and then, along with the entire carcass of each mouse, evaluated for gross lesions. The liver and a portion of the subcutaneous tumor from each mouse were fixed overnight in 10% formalin, then transferred to 70% ethanol and embedded in paraffin blocks. The remaining portion of each tumor was snap-frozen in liquid nitrogen and stored at −80°C until analysis by Western blotting. Tumor tissue sections (4 μm) were immunostained with antibodies against Ki67 as done previously (Sargeant et al., 2008). The percentage of Ki67-positive tumor cells was counted in 10 randomly chosen 400× fields from representative tumor samples from each experimental group. Liver tissue sections were stained with hematoxylin and eosin (H&E) and toluidine blue by standard procedures. All liver and tumor tissues were examined microscopically by a veterinary pathologist (A.S.).

Statistical Analysis. Differences in relative NF-κB activation in vitro and among group means of tumor volume in vivo were analyzed for statistical significance using one-way analysis of variance followed by the Neuman-Keuls test for multiple comparisons. Differences were considered significant at $P < 0.05$. Statistical analysis was performed using SPSS for Windows (SPSS, Inc., Chicago, IL).

Results

OSU-A9 Suppresses the Viability of Different HCC Cell Lines with Equal Potency Irrespective of Genetic Abnormalities. The antitumor effects of OSU-A9 and the parent compound indole-3-carbinol were assessed in three human HCC cell lines (PLC5, Huh7, and Hep3B) by MTT assay. Although these HCC cells are known to be resistant to cytotoxic drugs as a result of the lack of p53 function, Bcl-xL

overexpression, and/or constitutive NF-κB activation (Takehara et al., 2001; Chiao et al., 2002; Watanabe et al., 2002), they were highly and comparably susceptible to the antiproliferative effect of OSU-A9 with IC_{50} values of 2.8 ± 0.1, 3.2 ± 0.1, and 3.2 ± 0.1 μM for Hep3B, Huh7, and PLC5 cells, respectively (Fig. 1A). In contrast, the IC_{50} values for indole-3-carbinol-induced cell death in these HCC cell lines ranged from 200 to 250 μM, indicating an approximately 100-fold lower potency relative to OSU-A9.

Of these three cell lines, Hep3B cells were used to conduct the subsequent mechanistic and in vivo efficacy studies considering that they contain constitutively activated NF-κB, which confers the doxorubicin-resistant phenotype to these cells (Chiao et al., 2002). Several lines of evidence indicate that the antiproliferative effects of OSU-A9 and indole-3-carbinol in Hep3B cells were attributable, at least in part, to the induction of apoptosis. Western blot analysis showed a dose-dependent effect of both agents on facilitating PARP cleavage and cytochrome *c* release into the cytoplasm after 48-h treatment (Fig. 1B), with relative potencies paralleling those in suppressing cell viability. In addition, flow cytometric analysis revealed a dose-dependent increase in the relative proportion of the sub-G_1 population, indicative of apoptotic death, after a 48-h exposure to OSU-A9 (Fig. 1C).

We also assessed the dose-dependent effects of OSU-A9 and indole-3-carbinol on inducing autophagy in Hep3B cells by monitoring the conversion of LC3-II from LC3-I, an essential step for autophagosome formation (Kabeya et al., 2000).

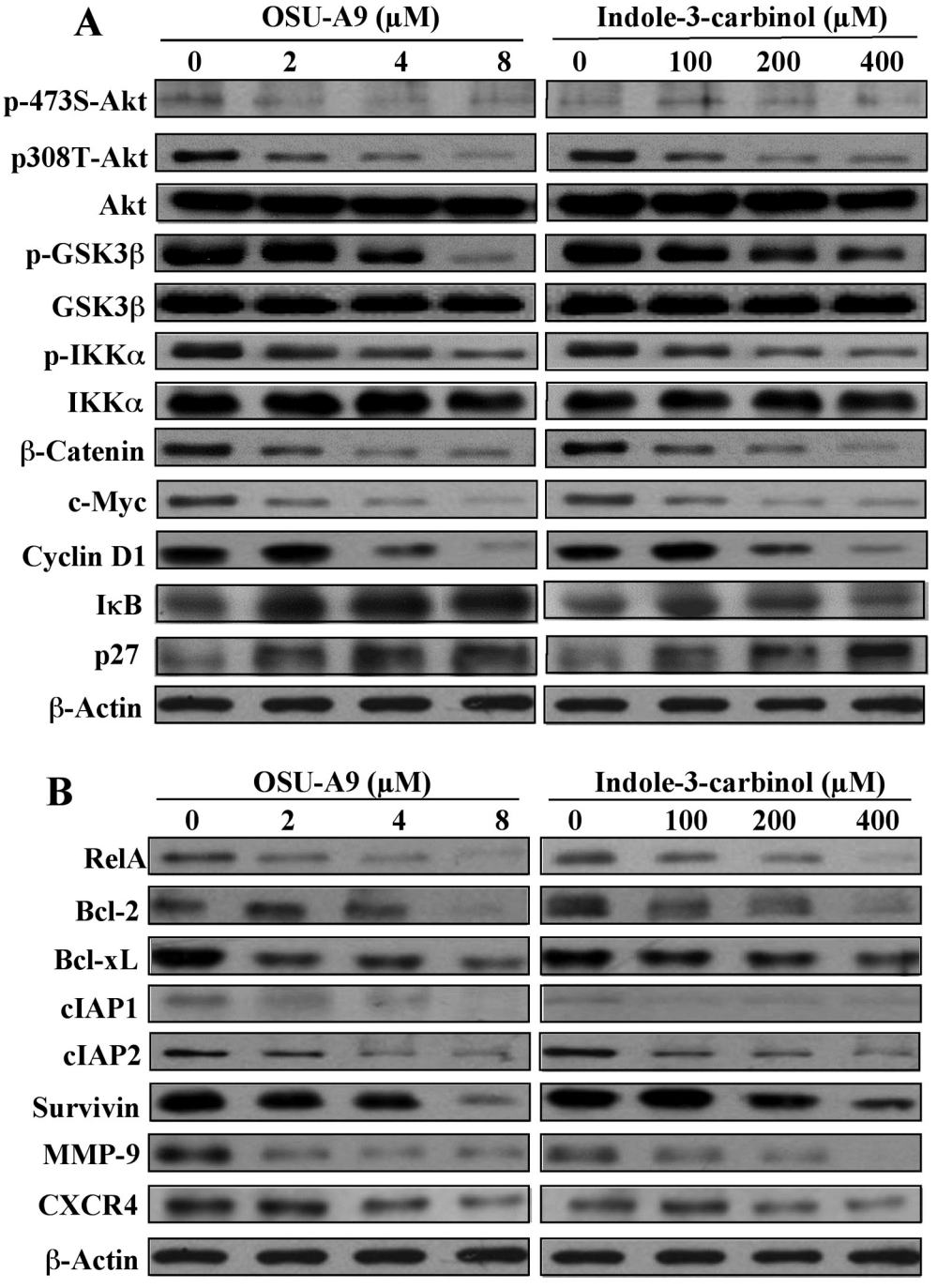

Fig. 2. Inhibition of the Akt-NF-κB signaling axis by OSU-A9 and indole-3-carbinol. A, Western blot analysis of the dose-dependent effects of OSU-A9 versus indole-3-carbinol on the phosphorylation of Akt and its downstream targets GSK3β, Bad, and IKKα, and the expression levels of β-catenin, c-Myc, cyclin D1, IκB, and p27 in Hep3B cells after 48-h exposure in 5% FBS-containing DMEM. B, Western blot analysis of the dose-dependent effects of OSU-A9 versus indole-3-carbinol on the expression levels of RelA/NF-κB p65 and various target gene products of NF-κB, including Bcl-2, Bcl-xL, cIAP1, cIAP2, survivin, MMP-9, and CXCR4, in Hep3B cells after 48-h exposure in 5% FBS-containing DMEM.

However, neither agent, even at high doses, gave rise to LC3-II formation, suggesting that autophagy did not play a role in OSU-A9- or indole-3-carbinol-induced cell death (Fig. 1D).

OSU-A9 Targets Akt Signaling. To shed light onto the effect of OSU-A9 on Akt signaling, we assessed the effects of OSU-A9 in relation to indole-3-carbinol on the phosphorylation/expression status of Akt and its downstream signaling targets. We have reported previously that although Hep3B cells exhibited low levels of p-Ser473-Akt as a result of functional phosphatase and tensin homolog, the phosphorylation level at Thr308 remained high (Hung et al., 2008). OSU-A9 showed potency in causing Akt inactivation that was 2 orders of magnitude higher than that of indole-3-carbinol, as manifested by the concomitant dose-dependent dephosphorylation of Thr308-Akt and two downstream kinase targets, glycogen synthase kinase (GSK)3β and IκB kinase (IKK)α (Fig. 2A). In contrast to IKKα, the dose-response effect for GSK3β dephosphorylation with OSU-A9 and indole-3-carbinol seemed to lag behind that of Akt in Hep3B cells. This discrepancy might be attributable to two factors: 1) basal levels of p-GSK3β elevated as a result of constitutive activation of the insulin-like growth factor signaling axis in Hep3B cells (Desbois-Mouthon et al., 2002) and 2) involvement of Akt-independent pathways in facilitating GSK3β phosphorylation, including those mediated by integrin-linked kinase (Troussard et al., 1999; Leung-Hagesteijn et al., 2001) and protein kinase Cζ, a downstream kinase effector of insulin-like growth factor signaling (Desbois-Mouthon et al., 2002).

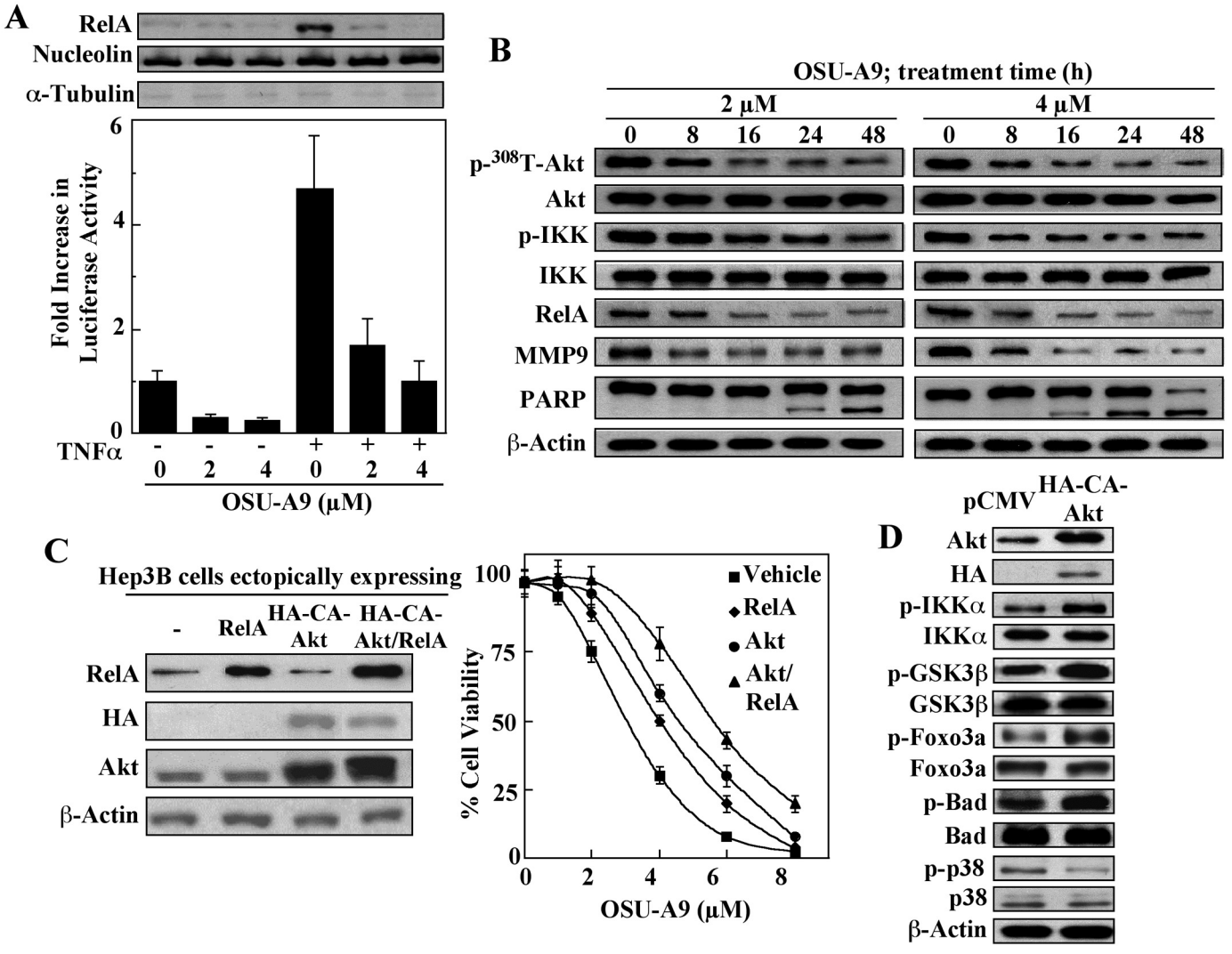

Fig. 3. Evidence that NF-κB signaling is inhibited by OSU-A9. A, top, Western blot analysis of the dose-dependent effect of OSU-A9 on TNFα-activated NF-κB nuclear translocation. Nuclear localization of RelA was determined by Western blotting after treatments. Nucleolin and α-tubulin were used as controls to ensure purity of nuclear fraction. Bottom, dose-dependent effect of OSU-A9 on TNFα-induced NF-κB-dependent transcriptional activity. Hep3B cells cotransfected with the pNF-κB-Luc reporter plasmid and *R. reniformis* luciferase control reporter vectors (pRL-CMV) were treated with the indicated concentrations of OSU-A9 with or without 10 ng/ml TNF-α. Luciferase activity as an indicator of NF-κB-dependent transcription was determined as described under *Materials and Methods*. Columns, mean; bars, S.D. (n = 3). B, Western blot analysis of the time-dependent effects of OSU-A9 at 2 and 4 μM on the phosphorylation/expression levels of proteins relevant to Akt and NF-κB signaling, including Akt, IKKα, RelA, and MMP9, and PARP cleavage in Hep3B cells in 5% FBS-supplemented DMEM. C, effect of ectopic expression of RelA and constitutively active (CA)-Akt on protecting Hep3B cells against OSU-A9-induced cell death. Left, Western blot analysis of the expression levels of RelA, hemagglutinin tag, and Akt in Hep3B cells transiently transfected with plasmids encoding RelA and/or CA-Akt relative to untransfected Hep3B cells. Right, dose-dependent effect of OSU-A9 on the viability of Hep3B cells ectopically expressing RelA and/or CA-Akt relative to untransfected Hep3B cells. Points, mean; bars, S.D. (n = 6). D, effect of ectopic expression of CA-Akt on the phosphorylation levels of its downstream targets IKKα, GSK3β, Foxo3a, and Bad and the stress-induced kinase p38 in Hep3B cells.

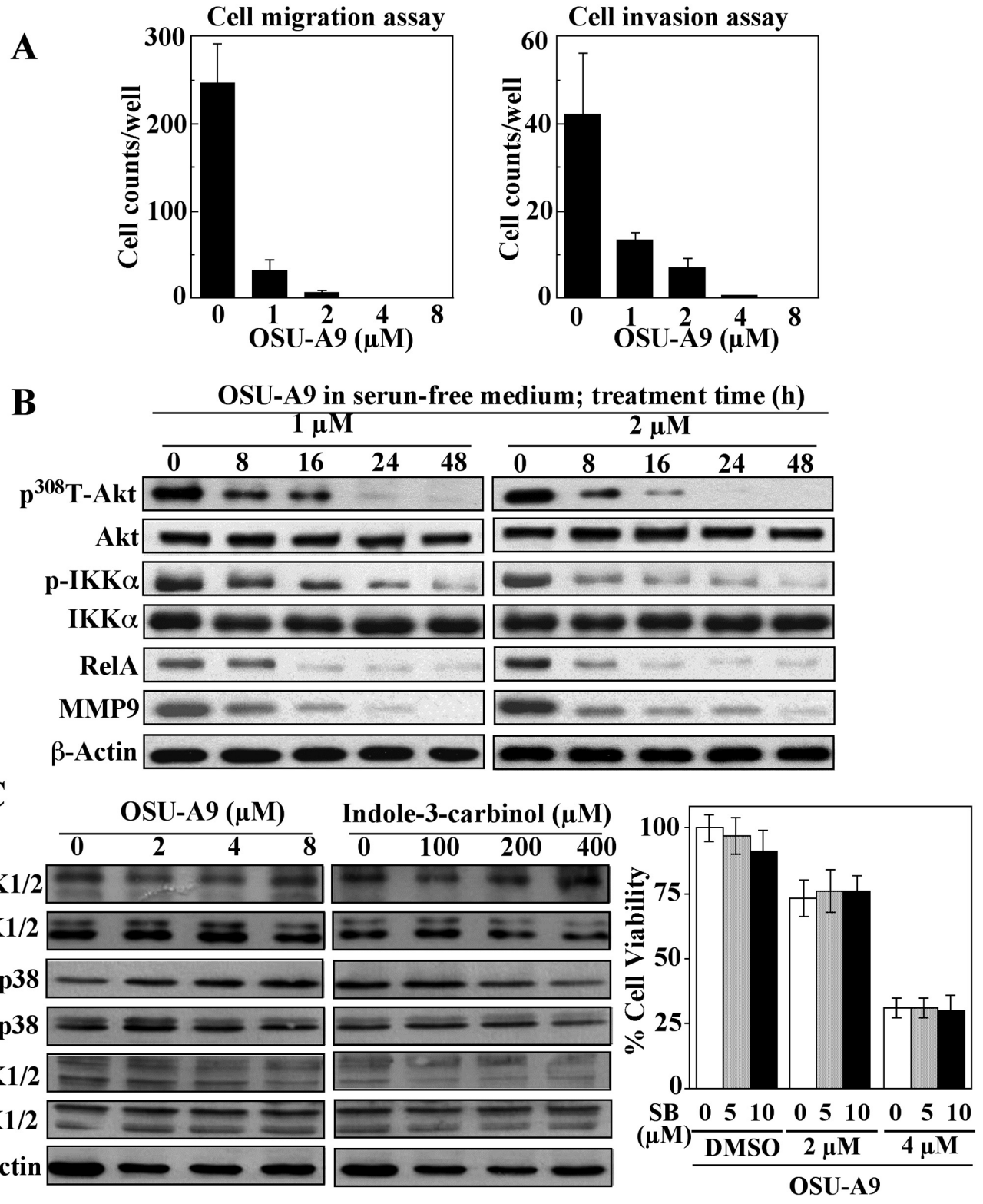

Fig. 4. Effects of OSU-A9 on modulating the migration, invasion, and the phosphorylation of MAP kinases of Hep3B cells. A, dose-dependent effects of OSU-A9 on Hep3B cell migration (left) and invasion (right). Boyden chamber assays of migration and invasion were performed as detailed under *Materials and Methods*. Columns, mean; bars, S.D. (n = 10). B, Western blot analysis of the time-dependent effects of OSU-A9 at 2 and 4 μM on the phosphorylation/expression level of proteins relevant to Akt and NF-κB signaling, including Akt, IKKα, RelA, and MMP9, in Hep3B cells in serum-free DMEM. C, Western blot analysis of the dose-dependent effect of OSU-A9 versus indole-3-carbinol on the phosphorylation of ERKs, p38, and JNKs in Hep3B cells after 48-h exposure in 5% FBS-containing DMEM. D, the p38 kinase inhibitor SB-203580 did not provide protection against OSU-A9-mediated inhibition of Hep3B cell viability in 5% FBS-containing DMEM after 48-h treatment. Columns, mean; bars, S.D. (n = 6).

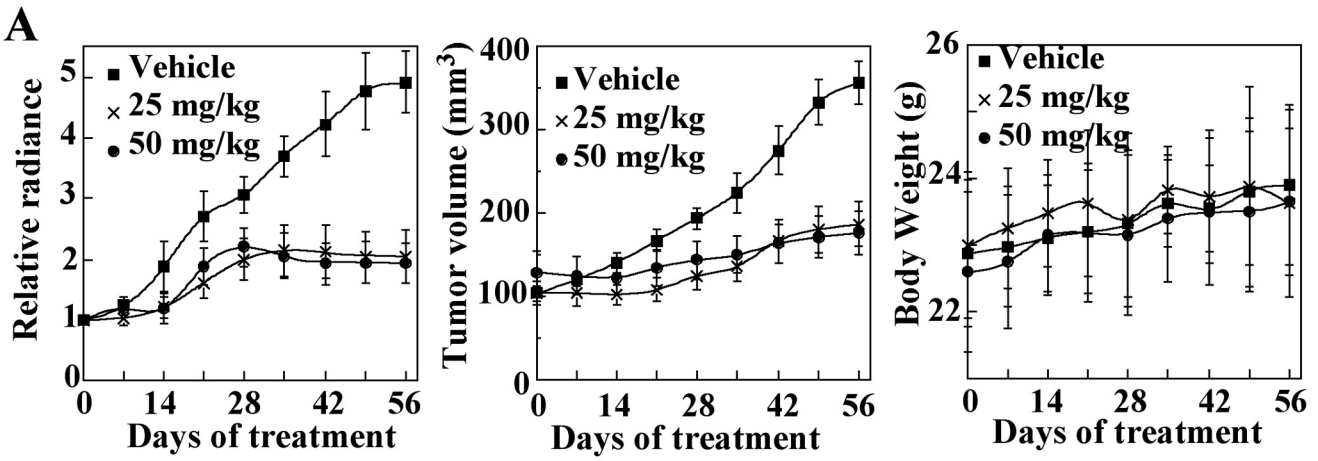

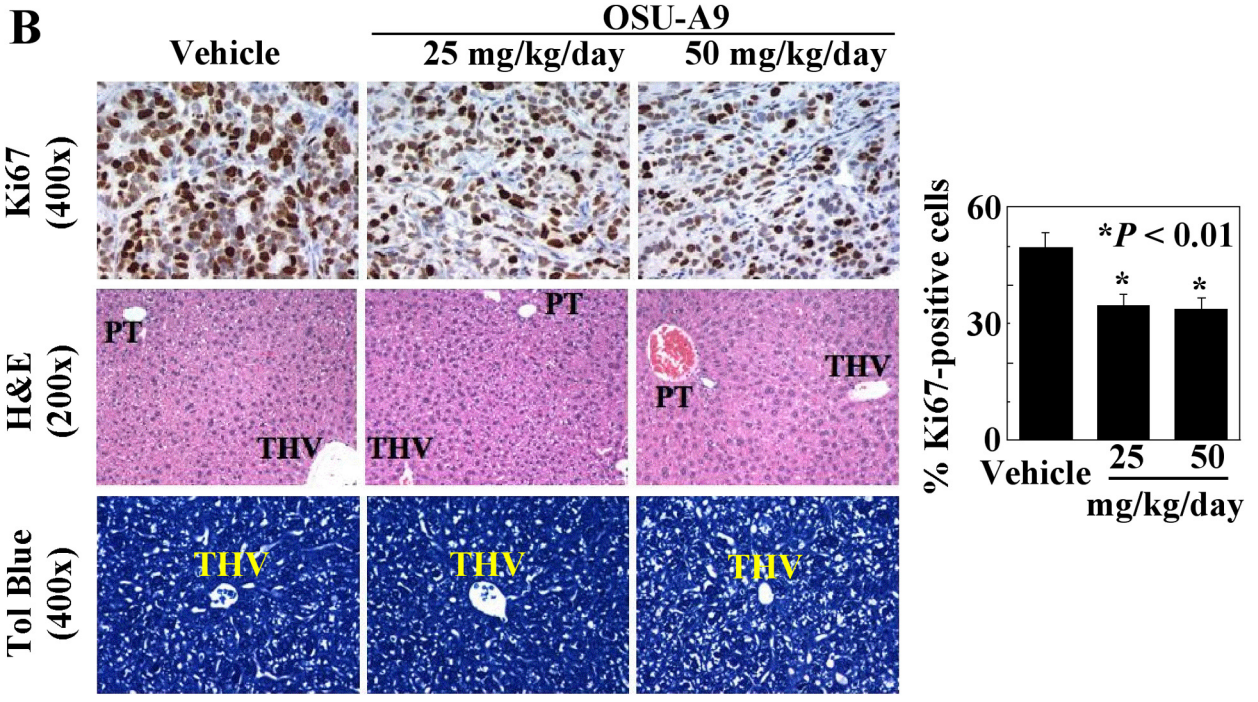

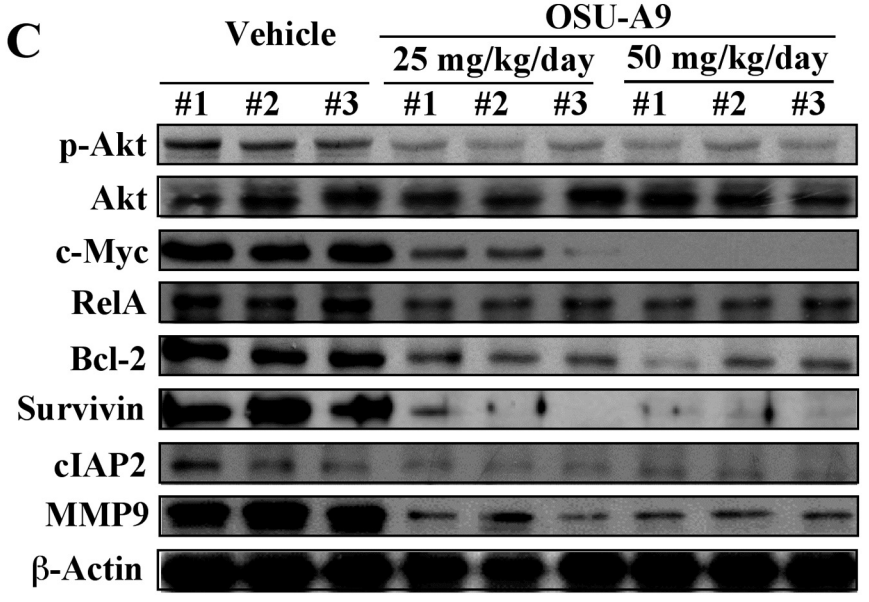

Nevertheless, the dephosphorylating activation of GSK3β might underlie the reduced expression levels of three key transcription factors, β-catenin and its target gene products cyclin D1 and c-Myc, all of which play a crucial role in HCC tumorigenesis and progression. In addition, the cell cycle regulatory protein p27 also showed a dose-dependent increase in expression in response to either agent, which is consistent with the previously reported link between drug-induced Akt inactivation and increased expression of this cyclin-dependent kinase inhibitor (Mitsuuchi et al., 2000; Sa and Stacey, 2004).

OSU-A9 Targets NF-κB Signaling. Our data indicate that OSU-A9 and indole-3-carbinol mediated the down-regulation of NF-κB signaling through two distinct mechanisms, albeit with a 100-fold difference in potency. First, the aforementioned Akt-dependent inactivation of IKKα by both agents led to the dose-dependent increase in the NF-κB inhibitor IκB in drug-treated cells (Fig. 2A). Second, these two agents share a unique ability to suppress the expression of the RelA/p65 NF-κB subunit (Fig. 2B). The concerted action of these two mechanisms accounts for the effective inhibition of NF-κB signaling by low micromolar concentrations of OSU-A9, as manifested by reductions in the expression of a series of NF-κB-regulated gene products involved in regulating cancer cell survival and metastasis, including Bcl-2, Bcl-xL, cIAP1, cIAP2, survivin, matrix metalloproteinase (MMP) 9, and CXCR4 (Fig. 2B). The ability of OSU-A9 to target NF-κB signaling was also demonstrated by the NF-κB-luciferase reporter gene assay, which shows the dose-dependent antagonism of TNFα-induced nuclear translocation of RelA and activation of NF-κB-dependent transcription by OSU-A9 (Fig. 3A).

OSU-A9, at 2 and 4 μM, mediated time-dependent changes in the functional status of Akt- and NF-κB-related signaling markers as early as 8 h after treatment in Hep3B cells, resulting in PARP cleavage at 24 and 16 h, respectively. The key role of Akt and NF-κB in OSU-A9's antiproliferative activity was underscored by the ability of ectopic expression of constitutively active Akt (CA-Akt) and RelA, each alone or in combination, to protect Hep3B cells from OSU-A9-induced cell death (Fig. 3C). The relative extents of protection were on the order of CA-Akt/RelA > CA-Akt > RelA. As indicated by the protection endowed by the double transfection of CA-Akt and RelA, the protective effect of RelA and that of CA-Akt were additive, indicating the involvement of Akt-dependent, NF-κB-independent apoptosis pathways in regulating OSU-A9-mediated cell death. This premise was borne out by the increased phosphorylation of many downstream targets of Akt in CA-Akt-expressing Hep3B cells, including GSK3β, the forkhead transcription factor FOXO3a, and the proapoptotic Bcl-2 family member Bad, all of which mediate NF-κB-independent survival pathways, accompanied by decreased phosphorylation of the stress-induced kinase p38 (Fig. 3D).

CXCR4 and MMP-9 have been shown to be up-regulated by NF-κB to promote aggressive tumor phenotypes (Karin and Greten, 2005). In light of the ability of OSU-A9 to suppress the expression of these two proteins (Fig. 2B), we examined its effects on Hep3B cell migration and invasion via Boyden chamber assays. As shown, OSU-A9 was highly effective, even at 1 μM, in mediating the inhibition of both processes, which seemed to be more potent than growth inhibition (IC_{50}, 2.8 μM). This discrepancy might be attributable to differences in the medium used (i.e., serum-free DMEM for migration/invasion assays versus 5% FBS-supplemented DMEM for MTT assays). We rationalized that serum-free medium would give rise to high potency because it was devoid of protein binding of drug molecules and growth factor-mediated stimulation of survival signaling pathways, including those mediated by Akt and NF-κB. This premise was corroborated by the higher potency of OSU-A9, at 1 and 2 μM, in blocking the functional status of Akt and NF-κB-related signaling proteins in serum-free conditions (Fig. 4B) relative to that in 5% FBS (Fig. 3B).

Relative to Akt and its downstream kinases, OSU-A9 and indole-3-carbinol did not cause significant changes in the phosphorylation levels of the three MAP kinases examined, including ERKs, p38, and JNK, in Hep3B cells, with the exception of increased expression of p-p38 in OSU-A9-treated cells (Fig. 4C, left). However, cotreatment with the p38 kinase inhibitor SB-203580 did not provide protection against OSU-A9-induced cell death (Fig. 4C, right). Increased p38 phosphorylation could be secondary to OSU-A9-induced Akt inactivation, because ectopic expression of CA-Akt decreased p-p38 levels in Hep3B cells (Fig. 3D). Together, these data argued against the role of any of these MAP kinases in OSU-A9-mediated apoptosis in Hep3B cells.

OSU-A9 Suppresses the Growth of HCC Xenograft Tumors in Vivo. Before evaluating in vivo antitumor efficacy, a pilot dose-range finding study was performed to identify a tolerable oral dose of OSU-A9 in mice. Tumor-free athymic nude mice were administered OSU-A9 as suspensions in vehicle at dose levels ranging from 5 to 100 mg/kg/day (n = 3 for each group) by gavage continuously for 14 days. None of these doses of OSU-A9 caused a weight loss of more than 10% at the end of treatment (data not shown). Doses of 50 and 25 mg/kg were selected for the subsequent efficacy study in Hep3B tumor-bearing mice.

To facilitate the assessment of tumor growth, Hep3B-luc cells were used to generate xenograft tumors in athymic nude mice. Athymic nude mice bearing established subcutaneous Hep3B-luc tumor xenografts (mean tumor volume ± S.E., 105 ± 7 mm^3) were treated once daily with oral OSU-A9 at 25 or 50 mg/kg or with vehicle by gavage for 56 days (n = 8). As shown in Fig. 5, assessments of tumor growth by both biolu-

Fig. 5. In vivo efficacy of oral OSU-A9. Athymic nude mice bearing luciferase-expressing Hep3B (Hep3B-Luc) xenograft tumors were treated orally with OSU-A9 at 25 and 50 mg/kg per day. Tumor burdens were determined by bioluminescent imaging and by direct measurement with calipers. A, suppressive effect OSU-A9 on the growth of established Hep3B-luc xenograft tumors in nude mice relative to that in vehicle-treated controls, as illustrated by changes in relative bioluminescence (left) and tumor volumes (middle). OSU-A9 did not cause losses in body weights of treated animals (right). Points, mean; bars, S.E. (n = 8). B, assessment of hepatotoxicity. Left, photomicrographs of representative Ki67-immunostained tumors (top row, 400× magnification), H&E-stained (middle row, 200× magnification), and toluidine blue-stained (bottom row, 400× magnification) sections of livers from mice treated as indicated. PT, portal triad; THV, terminal hepatic venule; Tol blue, toluidine blue. Right, proliferation indices of Hep3B-luc tumors from each treatment group, as determined by the percentage of Ki67-positive cells in representative tumor samples. *, $P < 0.01$. C, Western blot analysis of intratumoral biomarkers of drug activity in the homogenates of three representative Hep3B-luc tumors from each treatment group.

minescent imaging and direct caliper measurements demonstrated significant inhibition of Hep3B-luc tumor growth by OSU-A9. Treatment with 25 and 50 mg/kg daily inhibited tumor growth by 72 and 76%, respectively, as determined by bioluminescence (Fig. 5A, left), and by 67 and 80%, respectively, by direct measurement (Fig. 5A, middle), relative to vehicle-treated controls ($P < 0.01$). Moreover, tumor-bearing mice seemed to tolerate the long-term daily oral administration of OSU-A9 without overt signs of toxicity, as indicated by a lack of body weight losses (Fig. 5A, right), the absence of gross lesions at necropsy, and normal hematological and serum chemistry parameters (Supplemental Table 1).

The parent compound indole-3-carbinol is an inducer of the hepatic biotransformation enzymatic system, which occurs in association with centrilobular hepatocellular hypertrophy (Crowell et al., 2006), a morphologic marker of sustained enzyme induction in rodents (Grasso et al., 1991). Accordingly, liver tissue sections from the OSU-A9-treated mice were stained with H&E or toluidine blue and evaluated microscopically (Fig. 5B, left). No lesions were evident in the livers of drug-treated mice that exhibited a uniform size of hepatocytes across the hepatic lobule. Likewise, there were no apparent differences in toluidine blue staining among experimental groups. Because changes in toluidine blue staining can be used to distinguish the proliferation of smooth endoplasmic reticulum that occurs in association with enzyme induction (Sargeant et al., 2007), these results suggest that oral OSU-A9 is not a significant inducer of hepatic biotransformation enzymes.

The suppression of Hep3B-luc tumor growth by OSU-A9 was reflected in the significant reduction in the number of proliferating cells within the tumor, as determined by Ki67 immunostaining of tumor tissues (Fig. 5B, right). Moreover, to correlate the tumor-suppressive response observed in vivo with mechanisms identified in vitro, the effects of OSU-A9 on representative intratumoral biomarkers of drug activity were evaluated by immunoblotting of Hep3B-luc tumor homogenates collected after 56 days of treatment. Relative to the vehicle-treated controls, treatment with oral OSU-A9 markedly decreased Akt phosphorylation and the expression levels of c-Myc, RelA, Bcl-2, survivin, cIAP2, and MMP-9 (Fig. 5C), which represent hallmark biomarkers of drug-induced inhibition of Akt-NF-κB signaling in Hep3B-luc tumors. Together, these in vivo findings indicate the oral bioavailability, safety, and antitumor efficacy of OSU-A9.

Discussion

In this study, we demonstrated the translational potential of OSU-A9, a novel indole-3-carbinol derivative, to be developed into a new therapeutic agent for HCC. OSU-A9 induces apoptotic death in all three HCC cell lines tested at low micromolar concentrations irrespective of the molecular basis of their intrinsic resistance to cytotoxic agents such as doxorubicin. Reported cellular abnormalities associated with this resistant phenotype include loss of p53 function, Bcl-xL overexpression, and/or constitutive NF-κB activation (Takehara et al., 2001; Chiao et al., 2002; Watanabe et al., 2002).

Viewed from a mechanistic perspective, OSU-A9 displays a unique ability to interfere with the interplay between Akt- and NF-κB-mediated signaling pathways, leading to changes in the functional status of a wide array of signaling effectors pertaining to cell cycle arrest, apoptosis, angiogenesis, and metastasis (Fig. 6). Each of these signaling proteins, alone or in conjunction with other effectors, plays a role in the development and progression of HCC. For example, cyclin D1 is frequently overexpressed in HCC (Park et al., 2006), and a mutational activation of β-catenin has been reported in c-Myc and H-Ras transgenic mice that develop HCC (de La Coste et al., 1998). Moreover, the oncogenic cooperation between c-Myc and Bcl-2 causes continuous proliferation in the absence of mitogens (Pelengaris et al., 2002a,b). This broad range of action of OSU-A9 provides therapeutic advantages over many existing molecularly targeted drugs for HCC treatment. For example, HCC cells are generally resistant to gefitinib, an EGFR inhibitor, regardless of the expression levels of EGFR and basal activity of ERK1/2 and Akt (Okano et al., 2006). In addition, the proteasome inhibitor bortezomib was unable to induce apoptosis in PLC5 cells, due in part to its inability to down-regulate p-Akt (Chen et al., 2008).

Because HCC is a vascular tumor in which angiogenesis contributes to pathogenesis, the suppressive effect of OSU-A9 on the expression of CXCR4 and MMP-9 is noteworthy in light of their roles in tumor metastasis and angiogenesis (Balkwill, 2004). The strong correlation between CXCR4 expression and HCC progression (Schimanski et al., 2006) suggests CXCR4 as a viable target for HCC therapy. It has been reported that small interfering RNA-mediated silencing of CXCR4 blocked breast cancer metastasis (Liang et al., 2005), providing a proof-of-principle for this premise. In light of the pleiotropic mode of action of indole-3-carbinol in targeting multiple pathways, the

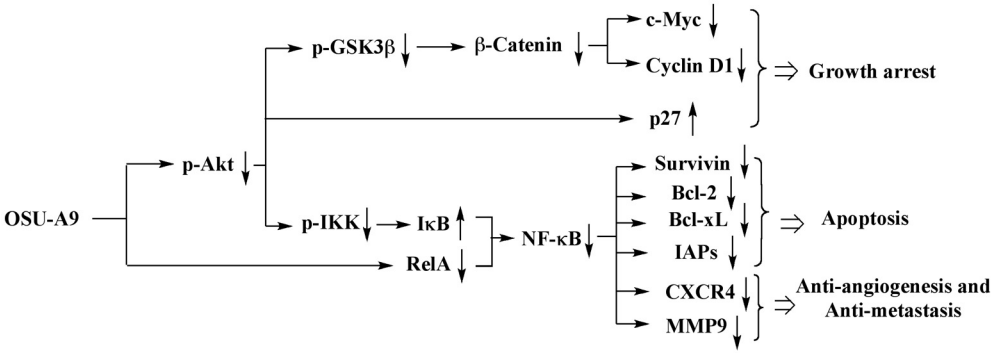

Fig. 6. Diagram depicting the effects of OSU-A9 on the Akt-NF-κB signaling axis. Through its ability to inhibit these two interactive signaling networks, OSU-A9 targets different facets of hepatocellular malignancy resulting in potent suppression of tumor growth and progression.

present study, however, could not exclude the involvement of Akt- and NF-κB-independent signaling targets in OSU-A9's antitumor effects. For example, a recent study has identified intracellular elastase as one possible direct target of indole-3-carbinol that leads to cell cycle arrest as a consequence of altered proteolytic processing of cyclin E in MDA-MB-231 breast cancer cells (Nguyen et al., 2008). This possible mechanism is currently under investigation in OSU-A9-treated HCC cells.

The in vivo findings revealed that a daily oral dose of OSU-A9 at 25 mg/kg produced maximal inhibition of Hep3B xenograft tumor growth without causing apparent toxicity. Equally important is that there were no changes in morphologic biomarkers of hepatotoxicity or cytochrome P450 enzyme induction, suggesting that OSU-A9 is not a significant inducer of the biotransformation enzymatic system. These findings are in contrast to those recently reported for indole-3-carbinol, which caused centrilobular hepatocellular hypertrophy and induced hepatic phase I and II enzymes in rodents (Yoshida et al., 2004; Crowell et al., 2006). These pathological changes underlie the controversy surrounding dietary indole-3-carbinol and increased incidences of uterine adenocarcinoma in animal models (Yoshida et al., 2004; Crowell et al., 2006).

In conclusion, our results show that the novel, orally bioavailable indole-3-carbinol derivative OSU-A9 potently inhibits HCC by targeting signaling pathways that regulate cancer cell survival and progression. These findings are consistent with, and extend, those previously reported for this agent in models of human prostate cancer (Weng et al., 2007). OSU-A9's broad spectrum of activity, which underlies its potent apoptogenic and antitumor activities, and its efficacy in models of multiple cancer types, support its clinical promise as a component of therapeutic strategies for human cancers, including advanced HCC, for which systemic therapies have been largely unsuccessful.

References

Arsura M and Cavin LG (2005) Nuclear factor-kappaB and liver carcinogenesis. *Cancer Lett* **229:**157–169.

Baba S, Cho SY, Ye Z, Cheng L, Engles JM, and Wahl RL (2007) How reproducible is bioluminescent imaging of tumor cell growth? Single time point versus the dynamic measurement approach. *Mol Imaging* **6:**315–322.

Balkwill F (2004) Cancer and the chemokine network. *Nat Rev Cancer* **4:**540–550.

Blum HE (2005) Hepatocellular carcinoma: therapy and prevention. *World J Gastroenterol* **11:**7391–7400.

Chen KF, Yeh PY, Yeh KH, Lu YS, Huang SY, and Cheng AL (2008) Down-regulation of phospho-Akt is a major molecular determinant of bortezomib-induced apoptosis in hepatocellular carcinoma cells. *Cancer Res* **68:**6698–6707.

Chiao PJ, Na R, Niu J, Sclabas GM, Dong Q, and Curley SA (2002) Role of Rel/NF-kappaB transcription factors in apoptosis of human hepatocellular carcinoma cells. *Cancer* **95:**1696–1705.

Chinni SR and Sarkar FH (2002) Akt inactivation is a key event in indole-3-carbinol-induced apoptosis in PC-3 cells. *Clin Cancer Res* **8:**1228–1236.

Crowell JA, Page JG, Levine BS, Tomlinson MJ, and Hebert CD (2006) Indole-3-carbinol, but not its major digestive product 3,3′-diindolylmethane, induces reversible hepatocyte hypertrophy and cytochromes P450. *Toxicol Appl Pharmacol* **211:**115–123.

de La Coste A, Romagnolo B, Billuart P, Renard CA, Buendia MA, Soubrane O, Fabre M, Chelly J, Beldjord C, Kahn A, et al. (1998) Somatic mutations of the beta-catenin gene are frequent in mouse and human hepatocellular carcinomas. *Proc Natl Acad Sci U S A* **95:**8847–8851.

Desbois-Mouthon C, Blivet-Van Eggelpoël MJ, Beurel E, Boissan M, Delélo R, Cadoret A, and Capeau J (2002) Dysregulation of glycogen synthase kinase-3beta signaling in hepatocellular carcinoma cells. *Hepatology* **36:**1528–1536.

El-Serag HB and Rudolph KL (2007) Hepatocellular carcinoma: epidemiology and molecular carcinogenesis. *Gastroenterology* **132:**2557–2576.

Grasso P, Sharratt M, and Cohen AJ (1991) Role of persistent, non-genotoxic tissue damage in rodent cancer and relevance to humans. *Annu Rev Pharmacol Toxicol* **31:**253–287.

Hu TH, Huang CC, Lin PR, Chang HW, Ger LP, Lin YW, Changchien CS, Lee CM, and Tai MH (2003) Expression and prognostic role of tumor suppressor gene PTEN/MMAC1/TEP1 in hepatocellular carcinoma. *Cancer* **97:**1929–1940.

Hung JH, Lu YS, Wang YC, Ma YH, Wang DS, Kulp SK, Muthusamy N, Byrd JC, Cheng AL, and Chen CS (2008) FTY720 induces apoptosis in hepatocellular carcinoma cells through activation of protein kinase C delta signaling. *Cancer Res* **68:**1204–1212.

Jenkins DE, Oei Y, Hornig YS, Yu SF, Dusich J, Purchio T, and Contag PR (2003a) Bioluminescent imaging (BLI) to improve and refine traditional murine models of tumor growth and metastasis. *Clin Exp Metastasis* **20:**733–744.

Jenkins DE, Yu SF, Hornig YS, Purchio T, and Contag PR (2003b) In vivo monitoring of tumor relapse and metastasis using bioluminescent PC-3M-luc-C6 cells in murine models of human prostate cancer. *Clin Exp Metastasis* **20:**745–756.

Kabeya Y, Mizushima N, Ueno T, Yamamoto A, Kirisako T, Noda T, Kominami E, Ohsumi Y, and Yoshimori T (2000) LC3, a mammalian homologue of yeast Apg8p, is localized in autophagosome membranes after processing. *EMBO J* **19:**5720–5728.

Karin M (2006) NF-kappaB and cancer: mechanisms and targets. *Mol Carcinog* **45:**355–361.

Karin M and Greten FR (2005) NF-kappaB: linking inflammation and immunity to cancer development and progression. *Nat Rev Immunol* **5:**749–759.

Kulp SK, Chen CS, Wang DS, Chen CY, and Chen CS (2006) Antitumor effects of a novel phenylbutyrate-based histone deacetylase inhibitor, (S)-HDAC-42, in prostate cancer. *Clin Cancer Res* **12:**5199–5206.

Leung-Hagesteijn C, Mahendra A, Naruszewicz I, and Hannigan GE (2001) Modulation of integrin signal transduction by ILKAP, a protein phosphatase 2C associating with the integrin-linked kinase, ILK1. *EMBO J* **20:**2160–2170.

Liang Z, Yoon Y, Votaw J, Goodman MM, Williams L, and Shim H (2005) Silencing of CXCR4 blocks breast cancer metastasis. *Cancer Res* **65:**967–971.

Mitsuuchi Y, Johnson SW, Selvakumaran M, Williams SJ, Hamilton TC, and Testa JR (2000) The phosphatidylinositol 3-kinase/AKT signal transduction pathway plays a critical role in the expression of p21WAF1/CIP1/SDI1 induced by cisplatin and paclitaxel. *Cancer Res* **60:**5390–5394.

Nakanishi K, Sakamoto M, Yamasaki S, Todo S, and Hirohashi S (2005) Akt phosphorylation is a risk factor for early disease recurrence and poor prognosis in hepatocellular carcinoma. *Cancer* **103:**307–312.

Nguyen HH, Aronchik I, Brar GA, Nguyen DH, Bjeldanes LF, and Firestone GL (2008) The dietary phytochemical indole-3-carbinol is a natural elastase enzymatic inhibitor that disrupts cyclin E protein processing. *Proc Natl Acad Sci U S A* **105:**19750–19755.

Okano J, Matsumoto K, Nagahara T, and Murawaki Y (2006) Gefitinib and the modulation of the signaling pathways downstream of epidermal growth factor receptor in human liver cancer cells. *J Gastroenterol* **41:**166–176.

Park SG, Chung C, Kang H, Kim JY, and Jung G (2006) Up-regulation of cyclin D1 by HBx is mediated by NF-kappaB2/BCL3 complex through kappaB site of cyclin D1 promoter. *J Biol Chem* **281:**31770–31777.

Pelengaris S, Khan M, and Evan G (2002a) c-MYC: more than just a matter of life and death. *Nat Rev Cancer* **2:**764–776.

Pelengaris S, Khan M, and Evan GI (2002b) Suppression of Myc-induced apoptosis in beta cells exposes multiple oncogenic properties of Myc and triggers carcinogenic progression. *Cell* **109:**321–334.

Rahman KM, Li Y, and Sarkar FH (2004) Inactivation of akt and NF-kappaB play important roles during indole-3-carbinol-induced apoptosis in breast cancer cells. *Nutr Cancer* **48:**84–94.

Rehemtulla A, Stegman LD, Cardozo SJ, Gupta S, Hall DE, Contag CH, and Ross BD (2000) Rapid and quantitative assessment of cancer treatment response using in vivo bioluminescence imaging. *Neoplasia* **2:**491–495.

Sa G and Stacey DW (2004) P27 expression is regulated by separate signaling pathways, downstream of Ras, in each cell cycle phase. *Exp Cell Res* **300:**427–439.

Sargeant AM, Klein RD, Rengel RC, Clinton SK, Kulp SK, Kashida Y, Yamaguchi M, Wang X, and Chen CS (2007) Chemopreventive and bioenergetic signaling effects of PDK1/Akt pathway inhibition in a transgenic mouse model of prostate cancer. *Toxicol Pathol* **35:**549–561.

Sargeant AM, Rengel RC, Kulp SK, Klein RD, Clinton SK, Wang YC, and Chen CS (2008) OSU-HDAC42, a histone deacetylase inhibitor, blocks prostate tumor progression in the transgenic adenocarcinoma of the mouse prostate model. *Cancer Res* **68:**3999–4009.

Scanga A and Kowdley K (2009) Sorafenib: A glimmer of hope for unresectable hepatocellular carcinoma? *Hepatology* **49:**332–334.

Scatena CD, Hepner MA, Oei YA, Dusich JM, Yu SF, Purchio T, Contag PR, and Jenkins DE (2004) Imaging of bioluminescent LNCaP-luc-M6 tumors: a new animal model for the study of metastatic human prostate cancer. *Prostate* **59:**292–303.

Schimanski CC, Bahre R, Gockel I, Müller A, Frerichs K, Hörner V, Teufel A, Simiantonaki N, Biesterfeld S, Wehler T, et al. (2006) Dissemination of hepatocellular carcinoma is mediated via chemokine receptor CXCR4. *Br J Cancer* **95:**210–217.

Suckow M, Danneman P, and Brayton C (2001) *The Laboratory Mouse*, CRC Press, Inc., Boca Raton, FL.

Takehara T, Liu X, Fujimoto J, Friedman SL, and Takahashi H (2001) Expression and role of Bcl-xL in human hepatocellular carcinomas. *Hepatology* **34:**55–61.

Troussard AA, Tan C, Yoganathan TN, and Dedhar S (1999) Cell-extracellular matrix interactions stimulate the AP-1 transcription factor in an integrin-linked kinase- and glycogen synthase kinase 3-dependent manner. *Mol Cell Biol* **19:**7420–7427.

Watanabe J, Kushihata F, Honda K, Mominoki K, Matsuda S, and Kobayashi N (2002) Bcl-xL overexpression in human hepatocellular carcinoma. *Int J Oncol* **21:**515–519.

Weng JR, Tsai CH, Kulp SK, and Chen CS (2008) Indole-3-carbinol as a chemopreventive and anti-cancer agent. *Cancer Lett* **262:**153–163.
Weng JR, Tsai CH, Kulp SK, Wang D, Lin CH, Yang HC, Ma Y, Sargeant A, Chiu CF, Tsai MH, et al. (2007) A potent indole-3-carbinol derived antitumor agent with pleiotropic effects on multiple signaling pathways in prostate cancer cells. *Cancer Res* **67:**7815–7824.
Yoshida M, Katashima S, Ando J, Tanaka T, Uematsu F, Nakae D, and Maekawa A (2004) Dietary indole-3-carbinol promotes endometrial adenocarcinoma development in rats initiated with *N*-ethyl-*N*′-nitro-*N*-nitrosoguanidine, with induction of cytochrome P450s in the liver and consequent modulation of estrogen metabolism. *Carcinogenesis* **25:**2257–2264.

Address correspondence to: Dr. Ching-Shih Chen, Division of Medicinal Chemistry, College of Pharmacy, The Ohio State University, 500 W. 12th Avenue, Columbus, OH 43210. E-mail: chen.844@osu.edu.